

Effect of Incident Light on Transport Properties of Pulsed Laser Deposited Manganite Thin Films

Pankaj Solanki^{1,3}, Pratik Lakhani², Ashish Raval³, Bharat Kataria^{3,*}

¹Department of Physics, Saurashtra University, Rajkot, Gujarat 360005, India

²Shantilal Shah Engineering College, Bhavnagar, Gujarat 364060, India

³Department of Nanoscience and Advanced Materials, Saurashtra University, Rajkot, Gujarat 360005, India

*Corresponding author: Email: brkataria22@rediffmail.com

DOI: 10.5185/amlett.2020.041502

In this communication, we report the results of different light illumination on electrical transport properties of $\text{La}_{0.67}\text{Ca}_{0.33}\text{Mn}_{0.9}\text{Ga}_{0.1}\text{O}_3$ (LCMGO) thin films grown on Si (100) (n-type phosphorus-doped) wafer using Pulsed Laser Deposition (PLD) System. The variation in deposition time changes the thickness of the films. X-ray Diffraction (XRD) reveals the polycrystalline structure of LCMGO thin films. The cross-sectional SEM were taken to determine the thickness of the films with changing deposition time. Atomic Force Micrographs (AFM) show that island type grains diffuse into one another to form a more uniform distribution of grains as the thickness of the film increases. The charge transport properties have been studied using the I-V measurement at LCMGO/Si interfaces. I-V measurement shows the backwards-diode like the behaviour of the LCMGO/Si p-n junction. The reverse bias current changes under the influence of different incident light illumination. The built-in electric field is generated at the interface when the film was illuminated with UV light. The tunnelling process for backward diode like p-n junction is explained using a modified Simmons model.

Introduction

Manganites are famous for their different properties and potential applications for a variety of devices and spintronic applications. Doped manganite materials show the different properties compared to pure/pristine manganite materials [1]. Pure manganite materials (i.e. LaMnO_3) are antiferromagnetic insulator with Mn^{3+} ions. Doping of $\text{Ca}^{2+}/\text{Sr}^{2+}$ force to change Mn^{3+} ions to Mn^{4+} ions with the equivalent number of dopant concentration. It causes the paramagnetic insulator to ferromagnetic metal transition following zener double exchange mechanism [2]. Manganite are highly sensitive to applied magnetic fields, electric current, electric field, incident light, applied pressures [3-5]. Manganite heterostructures show more prominent properties that bulk manganite materials can't, as the exchange energy and hopping energies are tuned at the interfaces [6]. Physical and Microstructural properties of manganite thin films are highly sensitive to the growth conditions, choice of substrate, deposition parameters [7, 8] etc. The growth conditions and deposition parameters change with the deposition techniques. There are several deposition techniques which are used to fabricate the thin films, Chemical Vapour Deposition (CVD) [8], Pulsed Laser Deposition (PLD) [9], Sputtering [10] etc. Manganite can be used in the potential applications for devices such as capacitors [9], sensors [11], resistive switching [12], transistors [13], p-n junctions [14], Memory storage Devices [15] etc.

Sun *et al.*, [16] have reported the photoelectric effect in temperature-dependent I-V characteristics of

$\text{La}_{0.29}\text{Pr}_{0.38}\text{Ca}_{0.33}\text{MnO}_3/\text{Nb-doped SrTiO}_3$ films and explained rectifying behaviour in the context of manganite materials the e_g band act as a valence band and t_{2g} as the conduction band (spin-up: valence band; spin-down: conduction band). The increment (below room temperature) in temperature makes the bandgap smaller. Panda *et al.*, [17] reported good rectifying behaviour of p- $\text{La}_{0.7}\text{Ca}_{0.3}\text{MnO}_3/\text{SrTiO}_3/\text{n-Si}$ and explained magneto-resistive property using standard spin injection mechanism in the magnetic p-n junction. Mona *et al.*, [18] have reported the rectifying behaviour of $\text{La}_{0.7}\text{Sr}_{0.3}\text{MnO}_3/\text{SiO}_2/\text{Si}$ heterojunction, discussed the role of the interface, and explained the Schottky type rectifying behaviour with "dead" layer of SiO_2 at an interface in the I-V characteristics. Zhao *et al.*, [19] have reported high-sensitivity photovoltaic response of $\text{La}_{0.4}\text{Ca}_{0.6}\text{MnO}_3/\text{Si}$ thin film deposited using sputtering technique and observed weak light detection properties with highly sensitive photo response application in the heterojunction prepared by wide-bandgap oxides and Si. Abad *et al.*, [20] have reported the existence of insulating layer at the surface of the as-grown LCMO film. Also reported the effect of annealing on the insulating layer, they successfully fitted the Simmons Model to understand the tunnelling process responsible for the charge conduction mechanism. Prashant *et al.*, [21] explained the transport mechanism of quasiparticle tunnelling, tunnelling through disordered metallic oxides and spin-flip scattering at grain boundary using the Simmons model for $\text{La}_{0.7}\text{A}_{0.3}\text{MnO}_3$ (A= Ca, Sr, Ba) thin films grown on LAO (100) substrate.

In the present case, we have studied the effect of incident light on LCMGO/Si thin films having various thicknesses in detail. I-V characteristics have been understood using the Simmons model.

Experimental

$\text{La}_{0.67}\text{Ca}_{0.33}\text{Mn}_{0.9}\text{Ga}_{0.1}\text{O}_3$ (LCMGO)/ Si thin films were deposited using the Pulsed Laser Deposition (PLD) technique. The target of LCMGO was prepared using conventional Solid State reaction (SSR) route [22]. The stoichiometry of $\text{La}_{0.67}\text{Ca}_{0.33}\text{Mn}_{0.9}\text{Ga}_{0.1}\text{O}_3$ was maintained using starting materials La_2O_3 , Ga_2O_3 , Ca_2CO_3 and MnO_2 . The LCMGO target was sintered at 1175°C for 24 hours with intermediate grinding and heating in air. The PLD parameters were set to laser energy- 250 mJ (Coherent Laser System made KrF excimer laser with 248 nm wavelength, Pulse Rate- 5 Hz, Substrate Temperature- 750°C , and partial oxygen pressure- 350 mTorr). Films were grown on n-type Si wafer (Phosphorus doped) with (100) orientation. The deposition time was kept 8 minutes (LCMGO-8), 16 minutes (LCMGO-16) and 24 minutes (LCMGO-24) to have different thickness of the films (at Department of Nanoscience and Advanced materials, Saurashtra University, Rajkot). The phase purity and crystal structures of samples were characterized by X-ray diffraction (PANalytical X'pert with Cu-K α (1.5406 Å) at Department of Physics, Saurashtra University, Rajkot. The cross-sectional SEM (Zeiss Merlin/VP compact model) were taken to study the thickness of grown films. To study the surface topography, the Atomic Force Micrographs (AFM) were taken in noncontact mode (NTEGRA Aura (NT-MDT) at FCIPT, Gandhinagar. To understand the charge transform behaviour of LCMGO/ Si films under the influence of different lights the I-V (coplanar mode) measurements were done in the range of -1V to +1V at room temperature using Keithley source meter at Department of Physics, Saurashtra University, Rajkot.

Results and discussion

Fig. 1 shows the XRD patterns for the Si Substrate and the growth of orthorhombic LCMGO/Si films without any detectable traces of impurity. The graph in side panel in **Fig. 1** shows the enlarged view of the most intense peak corresponding to Si substrate and LCMGO layer. The most intense peak is shifting towards the higher 2θ values show the release in the strain. The plot in **Fig. 2** shows the increment in cell volume as a function of deposition time, values of cell parameters are listed in **Table 1**.

Table 1. Values of refined unit cell parameters, cell volume for $\text{La}_{0.67}\text{Ca}_{0.33}\text{Mn}_{0.9}\text{Ga}_{0.1}\text{O}_3$ manganite films.

Sample	a (Å)	b (Å)	c (Å)	Cell Volume (Å) ³
LCMGO8	5.4337	7.5947	5.449	244.8656
LCMGO16	5.4189	7.6484	5.4577	266.1993
LCMGO24	6.6103	7.8895	6.1409	320.2599

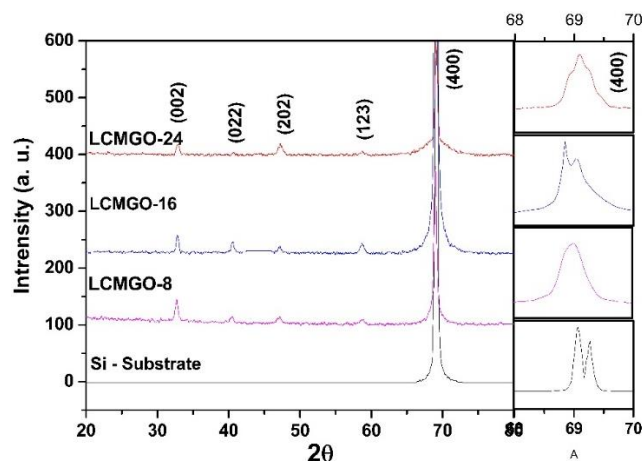


Fig. 1. XRD patterns for the Si Substrate and all three LCMGO/Si films.

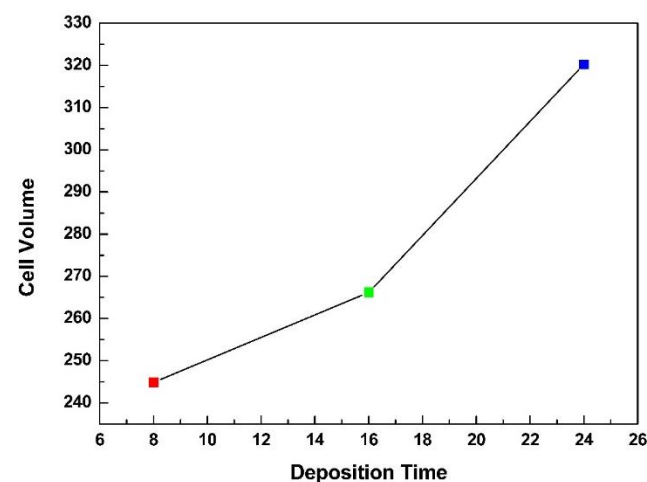


Fig. 2. Cell Volume as a function of deposition time.

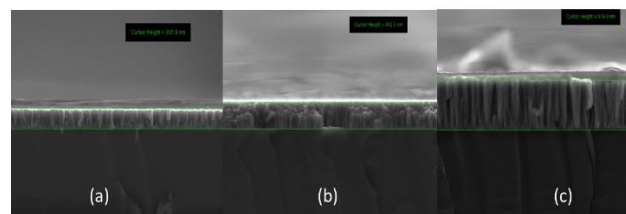


Fig. 3. Cross-sectional SEM micrographs of (a) LCMGO-8, (b) LCMGO-16 and (c) LCMGO-24 thin films.

Table 2. Thickness of the grown films.

Sample	Thickness (nm)
LCMGO-8	301.9
LCMGO-16	442.0
LCMGO-24	814.0

Fig. 3 shows the Cross-sectional SEM micrographs for all grown films. As shown in **Fig. 3** it is clear that the thickness of the films increases with increasing deposition time. The thicknesses of the films listed in **Table 2**. Atomic Force Micrographs (AFMs) were taken to understand the surface properties of deposited films.

Fig. 4 shows the AFM images of the LCMGO-8, LCMGO-16 & LCMGO-24 films. Increment in deposition time changes the surface morphology. The AFM images reveal the in-homogeneously distributed island type growth of LCMGO films on Si substrate. The LCMGO-8 has got both smaller islands as well as bigger islands type distribution of grains, whereas in LCMGO-16 more uniform size of islands type grains are formed. The island size appears comparatively larger than that of the LCMGO-8 which gets diffused into one another and have been replaced with parallel array type distribution. This may be attributed to the diffusion of the islands in one direction resulting in parallel stripe like arrangement.

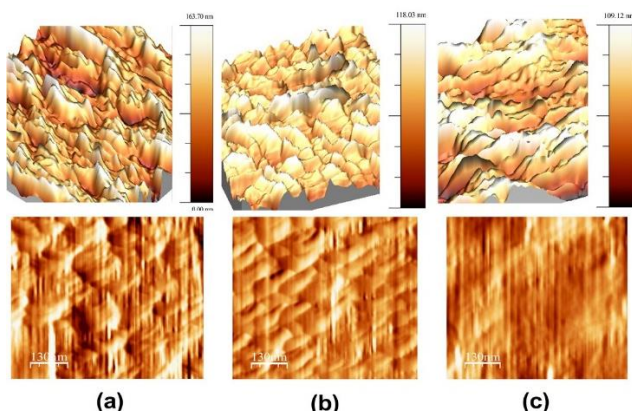


Fig. 4. AFM images for (a) LCMGO-8, (b) LCMGO-16 and (c) LCMGO-24 thin films.

Fig. 5 shows the I-V measurements for all LCMGO/Si films when illuminated with room light and UV light respectively. The inset image shows the enlarged view for forward-biased current. I-V measurement performed in -1V to +1V range reveals the electron-transport behaviour of LCMGO/Si p-n junction. From the I-V curves, it is clear that the LCMGO/Si junction shows the non-linear nature for all applied environment.

For the conventional p-n junction diode, normally forward current is much larger than that of the reverse current value. Some reports are available on the observation of large reverse current value than that of the forward current, so-called backward diode like behaviour. In the backward diode, the Fermi level is very close to the band edges, due to that the tunnelling of electrons increase rapidly from valance band of the p side into the conduction band of the n side when a small change in voltage is applied in reverse bias mode [23-25]

One noticeable feature of the presently studied I-V characteristics is large reverse-bias current compared to the forward bias current. Illumination of the films under room light increases the reverse bias current for all LCMGO/Si p-n junctions, with increasing voltage. Under the illumination of UV light, the reverse bias current slightly increases as compared to that of the room light illumination. As shown in insets of Fig. 4, forward bias currents are having very small changes as a function of voltage. It may be ascribed to the larger thickness dependent affinity of the

charge carriers that decrease as thickness of the films increases.

The energy of UV light is ~ 4.48 eV which is higher than the barrier height of LCMGO/Si p-n junction. The barrier height of LCMGO/Si p-n junction is ~3.9 eV, calculated using $\phi_0 = W_{\text{LCMGO}} - \phi_{\text{Si}}$ [26]. Where, W_{LCMGO} is the work function of the LCMGO (~ 4.88 eV) and ϕ_{Si} is the electron affinity of Si (~0.9 eV). The energy of incident light is higher than the barrier height; hence the charge carriers are generated and can easily cross-over the barrier, increasing the reverse-biased current. The bandgap of Si and LCMGO are reported to be 1.12 eV and 1.2 eV respectively, because of that the incidence of UV light is expected to produce photo-induced charge carriers at the interface of LCMGO/Si junction [27].

There are various theoretical models and mechanisms available to understand the charge transport behaviour of the materials, thermionic emission: $I = AT^2 \exp(-[\Phi_B - q(qV / 4\pi\epsilon_0\epsilon_d)^{1/2}] / KT)$ [14], hopping conduction mechanism: $I \propto V$ [14], Space Charge Limited conduction (SCLC) mechanism: $ISCLC = 9\mu\epsilon_r\epsilon_0\theta V^2 / 8d^3$ [26], (iv) Schottky barrier: $I = AT^2 \exp(-[\psi - (q^3V / 4\pi\epsilon_0k)^{1/2} / K_B T])$ [21], and (v) Simmons model : $I \propto V^n$ [27] etc. The Simmons model is best fitted in reverse bias mode of I-V characteristics for all the grown thin films.

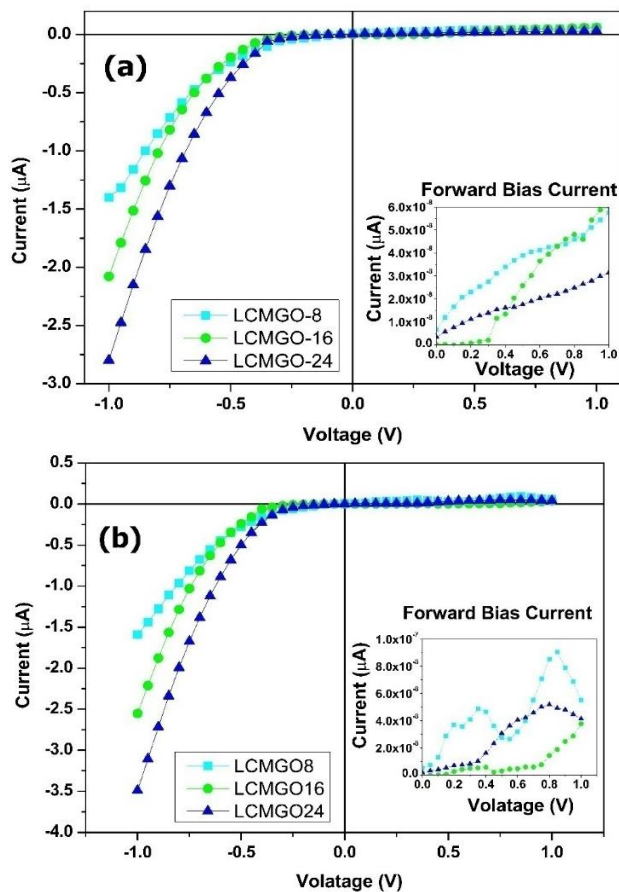


Fig. 5. I-V plots for all three, LCMGO-8/Si, LCMGO-16/Si, and LCMGO-24/Si thin films under the (a) room light and (b) UV light with having different thickness.

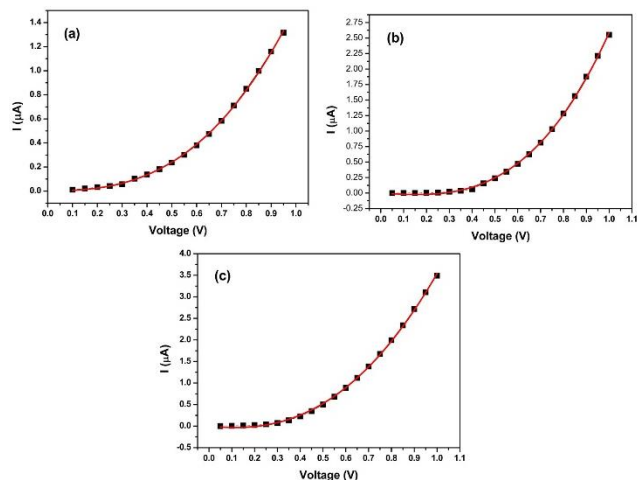


Fig. 6.1. Simmons Model Fitting in reverse bias mode for the all (a) LCMGO-8/Si, (b) LCMGO-16/Si and (c) LCMGO-24/Si under the room light.

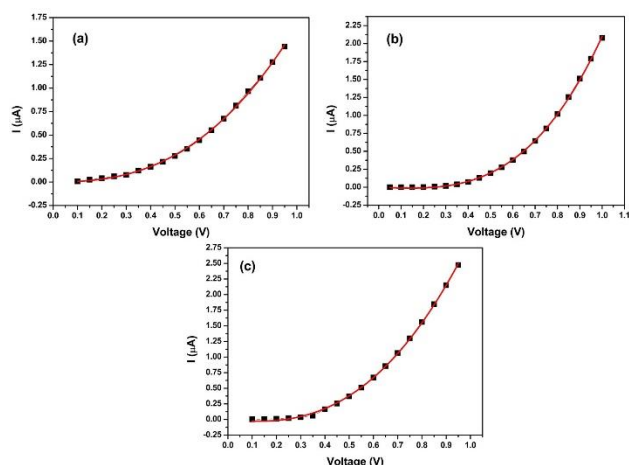


Fig. 6.2. Simmons Model Fitting in reverse bias mode for the all (a) LCMGO-8/Si, (b) LCMGO-16/Si and (c) LCMGO-24/Si under the UV light.

Fig. 6.1 and **Fig. 6.2** shows the fitting of the Simmons model for all the I-V curves under the illumination of room light and UV light respectively. Modified Simmons model was successfully fitted to all I-V curves using the equation $I = (\sigma \cdot V) + (k \cdot V^n)$, where, σ is the conductivity, k is a constant. Depending upon the interface barrier and power exponent n governing the charge transport mechanisms, value of n is important to understand the mechanism in the charge-transport behaviour of materials. For $n \geq 0.6$, tunnelling through disordered metallic oxides takes place, $n = 1.33$ corresponds to quasiparticle tunnelling via pairs of localized states and for $n > 1.4$, strong spin-flip scattering at an insulating barrier takes place [28]. Value of n for the present case are listed in **Table 3**.

Table 3. Values of n in the Simmons Model for all fitted curves.

Sample	LCMGO-8	LCMGO-16	LCMGO-24
ROOM LIGHT	2.56	3.09	2.54
UV LIGHT	2.74	2.97	2.39

The effect of thickness of deposited films on charge transport behaviour, illuminated with room light and UV light is shown in Fig. 5. It can be readily noticed that values of current is increasing with increasing thickness of LCMGO layer. This may be explained in terms of increasing thickness of the films. It tends to have a bulk analogue nature and the lattice strain is decreased between the LCGMO layer and Si substrate with increasing thickness, this may also be a reason why the islands are disappearing and the grains are arranged more orderly in LCGMO-24 films as seen in AFM images.

When the applied voltage increases, the electron of e_g levels are forced to move forward irrespective of spin scattering or the orientation of Mn ions [28]. In the formation of LCMGO/Si junction, the density of electrons and holes in LCMGO and Si should diffuse, this diffusion in electron-hole pair causes a built-in electric field in the space charge region at the interface of the LCMGO/Si film [27]. Under illumination of UV light, photo-induced charge carriers were separated because of the built-in electric field [29]. For the present case, the calculated value of the n for the Simmons model is greater than 1.4 for all I-V measurement, which confirms the generation of the built-in electric field at the interface. Theoretically, the strong spin-flip scattering of an electron at LCMGO/Si interface is responsible for the charge transport mechanism but under the influence of UV light, the built-in-electric field helps the charge carriers to crossover the interface. This may be the reason for the larger current in reverse bias mode as compared to that for the room light.

Conclusion

In conclusion, we have successfully grown the LCMGO/Si films having different thickness using Pulsed Laser Deposition (PLD) System. Growth of films was confirmed by the XRD patterns. Cross sectional SEM micrographs confirm the increment of thickness with increasing deposition time. AFM reveals the island type of growth of films on Si substrate which gets diffused and arranged more orderly and having homogeneous distribution of grain size as the thickness of film increases. I-V measurement confirms the backward diode like the behaviour of LCMGO/Si junction. As the energy of UV light is greater than the barrier height, it generates the built-in-electric field at the interface hence, more charge carriers can cross over the barrier as compared to the case of room light. The fitting of the Simmons model reveals the spin-flip scattering of e_g electrons at the insulating barrier of LCMGO/Si films. Spin flip scattering at the interface increases the tunnelling of charge carriers in reverse bias mode.

Acknowledgment

PPS and BRK acknowledge Dr. Mukesh Ranjan and Dr. C. Balasubramaniam, FCIPT, IPR, Gandhinagar for providing experimental facilities.

Keywords

Thin films, UV light, electron scattering, p-n junction, backward diode, modified simmons model.

Received: 10 January 2020

Revised: 15 March 2020

Accepted: 16 March 2020

Reference

1. Rao, C.N.R.; Mahesh, R.; Raychaudhari, A.K.; Mahendiran, R.; *J. Phys. Chem. Solid*, **1998**, *59*, 487.
2. Millis, A. J.; Littlewood, P. B.; Shraiman, B.I.; *Phys. Review Letter*, **1995**, *74*, 25.
3. Dagotto, E.; Hotta, T.; Moreo, A.; *Phys. Rep.*, **2001**, *344*, 1.
4. Salamon, M. B.; Jaime, M.; *Rev. Mod. Phys.* **2001**, *73*, 583.
5. Tokura, Y.; *Rep. Prog. Phys.*, **2006**, *69*, 797.
6. Mannhart, J.; Schlom, D. G.; *Science*, **2010**, *327*, 1607.
7. Parmar, R. N.; Markna, J. H.; Solanki, P. S.; Doshi, R. R.; Vachhani, P. S.; Kuberkar, D. G.; *J. of Nanoscience Nanotech.* **2008**, *8*, 4146.
8. Haghiri Gosnet, A.M.; Renard, J.P.; *J. Phys. D: Appl. Phys.* **2003**, *36*, 127.
9. Shang, D. S.; Wang, Q.; Chen, L. D.; Dong, R.; Li, X. M.; Zhang, W. Q.; *Physical Review B*, **2006**, *73*, 245427.
10. Zeng, X. T.; Wong, H. K.; *Applied Physics Letters*, **1995**, *66*, 3371.
11. Zhao, S. G.; Cheng, J. F.; Zhang, T.; Xie, Y.; Yan, X.L.; Liu, W.; Wang, J. Y.; Jin, K. X.; *Phys. B*, **2014**, *454*, 42.
12. Liu, X.; Biju, K.P.; Park, S.; Kim, I.; Siddik, M.; Sadaf S.; Hwang, H.; *Curr. Appl. Phys.* **2011**, *11*, e58.
13. Gajek, M.; Bibes, M.; Varela, M.; Fontcuberta, J.; Herranz, G.; Fusil, S.; Bouzehouane, K.; Barthelemy, A.; Fert, A.; *J. Appl. Phys.* **2006**, *99*, 1.
14. Khachar, Uma; Solanki, P.S.; Choudhary, R.J.; Phase, D.M.; Ganesan V.; Kuberkar, D.G.; *Solid State Commun.* **2012**, *152*, 34.
15. Levy, P.; Parisi, F.; Quintero, M.; Granja, L.; Curiale, J.; Sacanell, J.; Leyva G.; Polla, G.; *Phys. Rev. B*, **2002**, *65*, 140401(R), 1.
16. Sun, J. R.; Xiong, C. M.; Shen, B. G.; Wang, P. Y.; Weng, Y. X.; *Applied Physics Letters*, **2004**, *84*, 2611.
17. Panda, J.; Giri, S. K.; Nath, T. K.; *Materials Science and Engineering*, **2015**, *73*, 012134.
18. Mona, J.; Bertram, F.; Shukla, D. K.; Choudhary, R. J.; Kale, S. N.; Seeck, O. H.; *Appl. Sci. Lett.*, **2015**, *1*, 55.
19. Zhao, S. S.; Ni, H.; Zhao, K.; Zhao, S. Q.; Kong, Y. C.; Wong, H. K.; *Applied Optics*, **2011**, *50*, 17.
20. Abad, Ll; Martínez, B.; Valencia, S.; Gaupp, A.; Gudat W.; Balcells, Ll; *Advances in Science and Technology*, **2006**, *52*, 87.
21. Vachhani, P.S.; Solanki, P.S.; Markna, J.H.; Parmar, R.N.; Kuberkar, D.G.; *Indian Journals of Engineering & Material Science*, **2007**, *14*, 163.
22. Kataria, B.R.; Ravalía Ashish; Vyas, A.U.; Pandya, D.D.; Solanki, P.S.; Shah, N.A.; *Physica B: Condensed Matter*, **2018**, *545*, 182.
23. Sheng, Z.G.; Sun, Y.P.; Zhu, X.B.; Dai, J.M.; Song, W.H.; Yang, Z.R.; Hu L.; Zhang, R.R.; *J. Phys. D: Appl. Phys.*, **2008**, *41*, 135008.
24. Xiao, Y. S.; Zhang X. P.; Zhao, Y. G.; *Appl. Phys. Lett.*, **2006**, *88*, 213501.
25. Cui, Y.; Zhang, L.; Wang R.; Xie, G. L.; *Thin Solid Films*, **2008**, *516*, 2292.
26. Balcells, Ll.; Abad, Ll.; Rojas, I H.; Perez del Pino, A.; Estrade, S.; Arbiol, J.; Peiro, F.; Martinez, B.; *Jour. of Appl. Phy.*, **2008**, *103*, 07E303.
27. Liu, X. J.; Ni, H.; Zhao, K.; Zhao, S. Q.; Kong, Yu-Chau; Wong, H. K.; International Conference on Electronic & Mechanical Engineering and Information Technology, **2011**, *11*, 722.
28. Kambhala, Nagaiah; Viswanath P.; Angappane, S.; *Appl. Phys. Letters*, **2003**, *103*, 102408.
29. Xing, Jie; Jin, Kui-Juan; Lu, Huibin; a_ Meng He, Guozhen Liu, Jie Qiu, Yang, Guozhen; *Applied Physics Letters*, **2008**, *92*, 071113.